Journal of Alloys and Compounds 572 (2013) 5–10

Contents lists available at SciVerse ScienceDirect

Journal of Alloys and Compounds

journal homepage: www.elsevier.com/locate/jalcom

Microstructure and precipitates in annealed $Co_{38}Ni_{33}Al_{29}$ ferromagnetic shape memory alloy

J.B. Lu [a,*], H. Shi [a], S. Sedlakova-Ignacova [c], R. Espinoza [a], J. Kopeček [c], P. Sittner [c], B. Bártová [a,b], D. Schryvers [a]

[a] EMAT, University of Antwerp, Groenenborgerlaan 171, B-2020 Antwerp, Belgium
[b] CIME&LSME, École Polytechnique Fédérale de Lausanne, Station 12, Lausanne CH-1015, Switzerland
[c] Department of Functional Materials, Institute of Physics ASCR v.v.i., Na Slovance 2, Prague 8 CZ-182 21, Czech Republic

ARTICLE INFO

Article history:
Received 11 January 2013
Received in revised form 8 March 2013
Accepted 25 March 2013
Available online 2 April 2013

Keywords:
Ferromagnetic shape memory alloy
Precipitation
Microstructure
TEM
FIB/SEM

ABSTRACT

Transmission electron microscopy was performed to investigate the microstructure and precipitates in the annealed $Co_{38}Ni_{33}Al_{29}$ ferromagnetic shape memory alloy. Apart from the dendritic secondary phase in the austenite matrix, micron-sized (up to 100 μm) fcc-based precipitates with partial γ′ $L1_2$ ordering and containing none, one or three $\{1\,1\,1\}_p$ parallel twin planes were found. The orientation relationship between the precipitates and matrix was found to be Kurdjumov–Sachs. STEM–EDX analysis indicates that twinned and non-twinned precipitates are Co-rich and Al- and Ni-deficient with respect to the matrix and with a lower Co/Al ratio for the latter. The 3D morphologies of precipitates were reconstructed with focused ion beam/scanning electron microscope dual-beam slice-and-view imaging, showing that the single $\{1\,1\,1\}_p$ plane twinned precipitates have a plate-like shape while the non-twinned precipitates are lath-like and often bent.

1. Introduction

Shape memory alloys (SMAs) have attracted considerable attention because of their potential applications in industry as sensors and compact actuators and in medicine as self-expanding stents, orthodontic and orthopedic devices, etc. [1–3]. For conventional SMAs, the shape memory effect is induced by means of changes in either temperature or stress or both. In ferromagnetic shape memory alloys (FSMAs) the shape memory and related effects can be triggered not only by the temperature and stress, but also by changes in an external magnetic field [4].

One well-known shape memory system is paramagnetic Ni–Al in which the austenite β-phase has a cubic B2 structure [5]. With replacing Ni by Co this paramagnetic alloy changes into a ferromagnetic Co–Ni–Al SMA [6,7], which is also viewed as a high temperature SMA as a result of its increased transformation temperatures [8], an extra potential advantage over the conventional binary system. The B2 structure of the Co–Ni–Al austenite alloy undergoes a martenstic transformation into a tetragonal $L1_0$ martensitic phase [9]. The martensitic transformation temperatures (start M_s or other) and magnetic Curie temperature (T_c) can individually be controlled by changing the concentrations of Co and Al [6]. However, it is reported that Co–Ni–Al material only consisting of single β-phase exhibits very poor ductility [6]. The introduction of a eutectic secondary phase can improve the hot fabricability and the high temperature ductility [6,10,11], which implies an important advantage for practical applications. With these properties in mind the as-cast single crystal $Co_{38}Ni_{33}Al_{29}$ ferromagnetic SMA was studied by transmission electron microscopy (TEM) a few years ago [12]. Besides the eutectic secondary phase in the austenite matrix, nano-sized Co-rich precipitates were also observed, and the crystallographic relationship between larger nano-sized precipitates and matrix was found to be close to the Kurdjumow–Sachs (K–S) relationship. In order to investigate the evolution of the microstructure and precipitates influenced by different heat treatments, the as-cast samples were annealed at 1373 K for 72 h and followed by water quenching. On the other hand, in the Co–Ni–Al system it is also reported that the hardness of the alloy is affected by the heat treatment due to the presence of the precipitates [13]. From metallographic aspect, the shape, crystal structure and orientation relationship of precipitates play an important role in the behavior of the alloy. In the present study, the microstructure, morphology and chemical composition of the precipitates of the annealed sample will be investigated with conventional and analytical TEM. The 3D morphologies of different precipitates will also be revealed with focused ion beam (FIB)/scanning electron microscope (SEM) dual-beam slice-and-view imaging technique.

* Corresponding author. Tel.: +32 32653731.
E-mail address: jblu10@gmail.com (J.B. Lu).

0925-8388/$ - see front matter © 2013 Elsevier B.V. All rights reserved.
http://dx.doi.org/10.1016/j.jallcom.2013.03.228

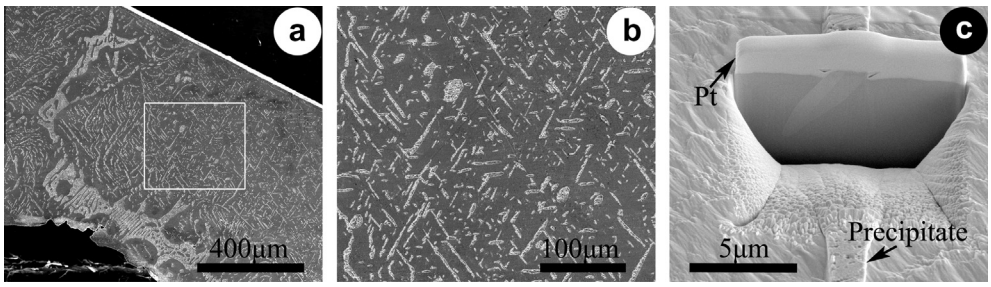

Fig. 1. (a) SEM image of the BM2 bulk sample revealing the overall microstructure of the alloy. (b) Enlarged image of the rectangle in (a) showing the distribution and surface cross-section morphologies (rod- and ellipse-like) of the precipitates in the matrix. (c) High magnification SEM image of a FIB cut from a precipitate revealing a plate-like morphology with a central interface.

2. Materials and methods

The $Co_{38}Ni_{33}Al_{29}$ ingot was obtained from Special Metals Corporation (New Hartford, NY). The ingot was melted and single crystals were grown by the directional Bridgman technique with a pulling rate of 7.7 μm s^{-1} in an Ar atmosphere [14]. The as-cast sample, labeled BM1, was then annealed at 1373 K in vacuum for 72 h and followed by water quenching. The annealed sample is labeled BM2 (see Table 1).

Conventional TEM samples were prepared by twin-jet electropolishing in a 20% sulfuric acid and 80% methanol electrolyte at 258 K [12]. The SEM observation, FIB cut and slice-and-view 3D imaging were carried out on an FEI Helios NanoLab 650 Dual Beam FIB/SEM system consisting of a standard ion column which allows Ga^+ cleaning and milling in a range of 500 V–30 kV. To clearly observe the microstructure of the bulk sample with SEM, the sample was etched in 50 ml H_2O, 50 ml HCl and 10 g $CuSO_4$ solution for 10 s. Conventional TEM was carried out on a LaB_6 Philips CM20, while the high-resolution TEM and analytical scanning TEM (STEM)–energy dispersive X-ray (EDX) analysis was performed on a FEI FEG Tecnai G^2, both microscopes operating at 200 kV.

3. Results

3.1. Transmission electron microscopy

The microstructure of the as-cast BM1 sample was studied before by conventional and advanced TEM [12]. Besides the dendritic secondary phases coexisting with the austenite matrix and grown from the eutectic phase transition, nano-sized precipitates ranging from 5 to 25 nm in diameter were observed. The orientation relationship between the larger of these nano-sized precipitates and the B2 matrix was confirmed to be close to the K–S relationship. The smaller precipitates were found to be faceted. Energy filtered TEM revealed that the precipitates are enriched in Co with respect to the matrix.

In the annealed BM2 sample, aside from the dendritic secondary phases dispersed in the austenite matrix, many micron-sized rod-like precipitates were found in the matrix and revealing a Widmanstätten-like structure as shown in the SEM image of Fig. 1a [9,15]. Fig. 1b shows the enlarged image of the rectangle in Fig. 1a. Apart from the rod-like precipitates, several ellipse-shaped (or elongated polygon) precipitates are observed. Moreover, at the left hand side of Fig. 1b, close to the eutectic structure, some curved rod-like precipitates can be seen. The precipitates in the BM2 sample are much larger than the ones in the BM1 sample, but their true 3D dimensions are difficult to judge from a simple SEM image. However, from the FIB cross-section of a straight rod-like precipitate shown in Fig. 1c they are estimated to have a plate-like shape several (5–10) μm wide, 1–2 μm thick and sometimes up to 100 μm long. From the contrast in this image it is also clear that a central interface exists parallel to the largest surface of the plate.

Fig. 2a shows the BF image of six relatively small precipitates in the BM2 sample. Selected area electron diffraction (SAED) in Fig. 2c–f confirm an fcc-based crystal structure for the precipitates. Moreover, weak ordering reflections are observed indicating at least partial γ′ $L1_2$ type ordering. The BF image in Fig. 2a was taken along the $[1\,1\,0]_p$ of precipitate-1 ("p" denotes the precipitate, "a" stands for the cubic austenite matrix). Four of the precipitates are labeled with numbers in order to illustrate their relative orientation relationships. Typical dimensions for these precipitates are 2 or 3 μm in thickness and a few microns in length (i.e., on the small end of the distribution scale when compared with the SEM image of Fig. 1). Fig. 2b shows the BF image of precipitate-1 at a higher magnification (several degrees off to the $[1\,1\,0]_p$ zone axis to enhance twin contrast) revealing a single $(-1\,1\,1)_p$ twin plane along the central axis. It is noted that precipitate-1 contains a re-entrant groove at one tip as indicated by the white arrow, which provides a preferential crystal growth site with low energy barrier for atom attachment [16–18]. Fig. 2c shows the corresponding SAED pattern of the twinning structure in Fig. 2b. Fig. 2d shows the SAED pattern taken along the $[1\,1\,0]_p$ zone axis of precipitate-1 from its interface with the austenite matrix as indicated by the black arrow in Fig. 2b. The latter confirms not only the K–S orientation relationship between the two structures i.e., $[1\,1\,1]_a//[1\,1\,0]_p$, $(-1\,1\,0)_a//(-1\,1\,1)_p$ but also shows that precipitate-1 is elongated along its $[1\text{–}12]_p$ direction (=$[-1\,-1\,2]_a$). Fig. 2e shows the SAED pattern from the region indicated by the white circle in Fig. 2b and thus consists of the diffraction patterns shown in Fig. 2c and d, i.e., containing the twinned precipitate as well as the austenite matrix. Fig. 2f shows the diffraction pattern taken from the area as indicated by the white circle in Fig. 2a containing the twinned precipitate-1, twinned precipitate-4 and austenite matrix. The white arrows in Fig. 2f indicate the diffraction spots from the twinning structures of both precipitates. From Fig. 2f we can measure an angle of 60° between the twin planes of precipitate-1 and -4, confirming the measurement in Fig. 2a. Twin plane orientation relationships between precipitates-1, -2 and -3 were also examined from their diffraction patterns relative to the diffraction pattern of the matrix, confirming the correspondence of the $\{1\,1\,1\}_p$ twin planes with the corresponding $\{1\,1\,0\}_a$ austenite planes as well as the full K–S orientation relationship. The contrast inside the long unlabeled precipitate also observed in Fig. 2a indicates a twin plane inclined to the viewing direction, which was confirmed after tilting the specimen. From the relative orientation relationships, it can thus be concluded that the twinned rod-shaped precipitates in the BM2 sample have a specific orientation distribution, possibly due to the existence of the $\{1\,1\,1\}_p$ twin planes inside the precipitates, while the precipitate and matrix crystal structures have a K–S orientation relationship.

Although most of the γ′ precipitates contain only one single twinning plane, Fig. 3a shows the $[1\,1\,0]_p$ (=$[1\,1\,1]_a$) zone axis BF image of a precipitate containing three parallel $\{1\,1\,1\}_p$ twinning planes. The corresponding SAED pattern taken from the whole area, i.e. including the surrounding matrix, is shown in the lower-right corner and is similar to the SAED in Fig. 2e. The inset in the lower-left corner shows the enlarged image of the lower-left